JOURNAL OF THEORETICAL
AND APPLIED MECHANICS
51, 1, pp. 143-158, Warsaw 2013

THREE-DIMENSIONAL ASYMMETRIC THERMO-ELASTIC ANALYSIS OF A FUNCTIONALLY GRADED ROTATING CYLINDRICAL SHELL

R. Akbari Alashti, M. Khorsand, M.H. Tarahhomi
Babol University of Technology, Mechanical Engineering Department, Babol, Iran
e-mail: raalashti@nit.ac.ir

In this paper, asymmetric deformation and stress analysis of a functionally graded hollow cylindrical shell under the effect of thermo-mechanical loads using the differential quadrature method is carried out. Without losing the generality, material properties of the cylindrical shell are assumed to be graded in the radial direction obeying a power law, while the Poisson ratio is assumed to be constant. The governing partial differential equations are expressed in terms of displacement and thermal fields in series forms with the help of two versions of differential quadrature methods, namely the polynomial and Fourier quadrature methods. The cylindrical shell is considered under both axisymmetric and asymmetric loading conditions. Numerical results for the axisymmetric loading condition of the cylindrical shell graded according to a power law function are obtained and compared with exact solutions which are found to be in very good agreement. Asymmetric thermo-elastic analysis of the shell rotating at a constant angular velocity is made and the effect of the grading parameter, angular velocity, temperature difference and geometry on stresses, radial displacement and temperature fields are presented.

Key words: functionally graded material, rotating cylindrical shell, differential quadrature, thermoelasticity

1. Introduction

A functionally graded material (FGM) is an inhomogeneous composite material at microscopic scale with the composition function that is designed to vary continuously within the solid. The mechanical and thermal responses of materials with spatial gradients in composition are of considerable interests in numerous industrial applications such as tribology, biomechanics, nanotechnology and high temperature technologies. These materials are usually mixtures of metal and ceramic which exhibit excellent thermal resistance with low levels of thermal stresses. These materials were first introduced by some Japanese Scientists in 1984 as ultra light temperature resistant materials for space vehicles (1993). Suresh and Mortensen (1998) presented the fundamentals of FG materials.

Two-dimensional higher-order deformation theory for the evaluation of displacements and stresses in FG plates subjected to thermal and mechanical loadings was presented by Matsunaga (2009). He employed the method of power series expansion of displacement components and several sets of truncated approximations to solve the static boundary value problem. Wu *et al.* (2005) investigated thermal buckling in the axial direction of cylindrical shells made of FG materials based on Donnell's shell theory and obtained their closed form solutions. Sofiyev (2007) presented closed form solutions of the thermal buckling loads of truncated conical shells made of an FG material, using the modified Donnell type dynamic stability and Galerkin's method. Pelletier and Vel (2006) analyzed the steady state response of an FG thick cylindrical shell subjected to thermal and mechanical loads and simply supported boundary conditions employing the power series method to solve the ordinary differential equations. Arciniega and Reddy (2007) presented geometrically nonlinear analysis of an FG shell using the first-order shell

theory and high-order Lagrangian interpolation functions. Bahtui and Eslami (2007) employed the second-order shear deformation shell theory, the Galerkin finite element formulation in the space domain and the Laplace transform in the time domain to formulate and obtain the thermoelastic response of an FG circular cylindrical shell subjected to thermal shock loading. Jabbari *et al.* (2002) presented a direct method of solution of the Navier equation for the general thermoelastic analysis of a hollow thick FG cylinder under the effect of one-dimensional steady state temperature distribution as a function of the radial coordinate. Zhao and Liew (2011) carried out free vibration analysis of a conical shell with material properties varying continuously through the thickness according with a power-law distribution function, using the element-free kp-Ritz method.

Peng and Li (2010) presented an analytical method to investigate steady state thermal stresses and radial displacement in FG disks by reducing the associated boundary value problem to a Fredholm integral equation. Afsar and Go (2010) formulated a thermo-elastic axisymmetric problem of a thin FG circular disk, leading to a second order ordinary differential equation which was solved by the finite element method. Hojjati and Jafari (2008) employed homotopy perturbation and Adomian's decomposition methods to obtain distributions of stresses and displacements in rotating annular elastic disks with uniform and variable thicknesses and densities. Bayat *et al.* (2007) carried out thermo-elastic analysis of an FG rotating disk with axisymmetric bending and steady-state thermal loading, using the first-order shear deformation Mindlin plate and von Karman theories. Shahzamanian *et al.* (2010) presented a finite element thermo-elastic analysis of the contact problem of a rotating brake disk made of a material functionally graded according to a power law function. Akbari alashti and Khorsand (2011) carried out three-dimensional thermo-elastic analysis of an FG cylindrical shell with piezoelectric layers under the effect of asymmetric thermo-electro-mechanical loads, using two versions of the differential quadrature methods, i.e. the polynomial and Fourier quadrature methods.

In this paper, three-dimensional asymmetric stress and deformation analysis of an FG hollow circular cylindrical shell under the effect of thermo-mechanical loads are carried out with the help of the Fourier and polynomial differential quadrature methods. Numerical solutions of stress, displacement and temperature fields in an FG cylindrical shell rotating at a constant angular velocity are obtained. Numerical results are compared with exact solutions for material properties defined by the power law which are found to be in good agreement. The effect of variation of material grading parameters, temperature variation, angular velocity and the geometry of the cylindrical shell on the distribution of stress, displacement and temperature fields are investigated.

2. Governing equations

A cylindrical shell made of an FG material with the inner radius of a, and the outer radius of b, is considered. A schematic view of the shell under study and the corresponding cylindrical coordinate system, i.e. r, θ and z-coordinates are shown in Fig. 1. The cylindrical shell is assumed to be isotropic and rotating at a constant angular velocity ω and subjected to mechanical and thermal loadings. Material properties of the shell, i.e. thermal and elastic constants are assumed to be independent of temperature and vary along the radial direction according to the following general formula

$$Y = Y(r) \tag{2.1}$$

where $Y(r)$ represents a material parameter of the shell such as the mass density ρ, Young's modulus E, Poisson's ratio ν, thermal expansion coefficient α and thermal conductivity coefficient K.

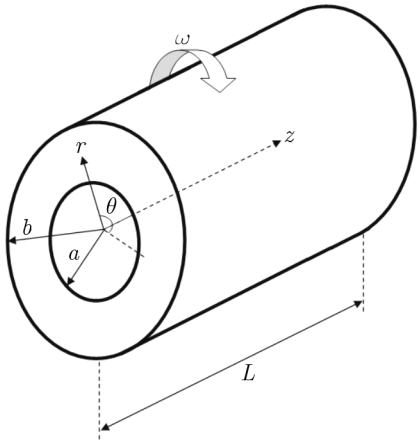

Fig. 1. Geometry and coordinates of the cylindrical shell

In this work, a three-dimensional thermo-elastic analysis of a cylindrical shell is carried out. The governing equations of the shell in three-dimensions and in presence of body forces are defined as

$$\begin{aligned}
&\frac{\partial \sigma_r}{\partial r}+\frac{1}{r}\frac{\partial \tau_{r\theta}}{\partial \theta}+\frac{\partial \tau_{rz}}{\partial z}+\frac{\sigma_r-\sigma_\theta}{r}+F_r=0 \qquad \frac{\partial \tau_{r\theta}}{\partial r}+\frac{1}{r}\frac{\partial \sigma_\theta}{\partial \theta}+\frac{\partial \tau_{\theta z}}{\partial z}+2\frac{\tau_{r\theta}}{r}+F_\theta=0\\
&\frac{1}{r}\frac{\partial \tau_{\theta z}}{\partial \theta}+\frac{\partial \sigma_z}{\partial z}+\frac{\partial \tau_{rz}}{\partial r}+\frac{1}{r}\tau_{rz}+F_z=0
\end{aligned} \tag{2.2}$$

And the linear strain displacement relations are

$$\begin{aligned}
&\varepsilon_{rr}=\frac{\partial u}{\partial r} && \varepsilon_{\theta\theta}=\frac{u}{r}+\frac{1}{r}\frac{\partial v}{\partial \theta} && \varepsilon_{zz}=\frac{\partial w}{\partial z}\\
&\varepsilon_{r\theta}=\frac{1}{2}\Big(\frac{1}{r}\frac{\partial u}{\partial \theta}+\frac{\partial v}{\partial r}-\frac{v}{r}\Big) && \varepsilon_{z\theta}=\frac{1}{2}\Big(\frac{\partial v}{\partial z}+\frac{1}{r}\frac{\partial w}{\partial \theta}\Big) && \varepsilon_{rz}=\frac{1}{2}\Big(\frac{\partial u}{\partial z}+\frac{\partial w}{\partial r}\Big)
\end{aligned} \tag{2.3}$$

The thermo-elastic constitutive equations describing the relation between the strain and the stress fields take the following form

$$\sigma_{ij}=\frac{E}{1+\nu}\varepsilon_{ij}+\frac{E\nu}{(1+\nu)(1-2\nu)}\varepsilon_{kk}\delta_{ij}-\frac{E\alpha T}{1-2\nu}\delta_{ij} \tag{2.4}$$

By substituting Eq. (2.3) into Eq. (2.4), components of the stress field are defined in terms of the displacement and temperature fields, and further substitution of stress components into Eq. (2.2) lead to the governing equations of equilibrium in terms of displacement and temperature fields of the shell. The corresponding differential equations in the three-direction form are found to be

$$\begin{aligned}
&\frac{\partial E}{(1+\nu)(1-2\nu)\partial r}\Big[(1-\nu)\frac{\partial u}{\partial r}+\nu\Big(\frac{u}{r}+\frac{1}{r}\frac{\partial v}{\partial \theta}\Big)+\nu\frac{\partial w}{\partial z}\Big]-\frac{\partial E}{(1-2\nu)\partial r}\alpha T\\
&\quad+\frac{E}{(1+\nu)(1-2\nu)}\Big[(1-\nu)\frac{\partial^2 u}{\partial r^2}+\nu\Big(\frac{1}{r}\frac{\partial u}{\partial r}-\frac{u}{r^2}+\frac{1}{r}\frac{\partial^2 v}{\partial r\partial \theta}-\frac{1}{r^2}\frac{\partial v}{\partial \theta}\Big)+\nu\frac{\partial^2 w}{\partial r\partial z}\Big]\\
&\quad-\frac{E\alpha}{1-2\nu}\frac{\partial T}{\partial r}-\frac{\partial \alpha}{(1-2\nu)\partial r}ET+\frac{E}{2(1+\nu)r}\Big(\frac{1}{r}\frac{\partial^2 u}{\partial \theta^2}+\frac{\partial^2 v}{\partial r\partial \theta}-\frac{1}{r}\frac{\partial v}{\partial \theta}\Big)
\end{aligned}$$

$$
\begin{aligned}
&+\frac{E}{2(1+\nu)}\Big(\frac{\partial^2 u}{\partial z^2}+\frac{\partial^2 w}{\partial r\partial z}\Big)+\frac{E}{(1+\nu)(1-2\nu)r_i}\Big\{\Big[(1-\nu)\frac{\partial u}{\partial r}+\nu\Big(\frac{u}{r}+\frac{1}{r}\frac{\partial v}{\partial\theta}\Big)+\nu\frac{\partial w}{\partial z}\Big]\\
&-\Big[(1-\nu)\Big(\frac{u}{r}+\frac{1}{r}\frac{\partial v}{\partial\theta}\Big)+\nu\frac{\partial u}{\partial r}+\nu\frac{\partial w}{\partial z}\Big]\Big\}+\rho r\omega^2=0\\
&\frac{\partial E}{2(1+\nu)\partial r}\Big(\frac{1}{r}\frac{\partial u}{\partial\theta}+\frac{\partial v}{\partial r}-\frac{v}{r}\Big)+\frac{E}{2(1+\nu)}\Big(\frac{1}{r}\frac{\partial^2 u}{\partial r\partial\theta}-\frac{1}{r^2}\frac{\partial u}{\partial\theta}+\frac{\partial^2 v}{\partial r^2}-\frac{1}{r}\frac{\partial v}{\partial r}+\frac{v}{r^2}\Big)\\
&+\frac{E}{(1+\nu)(1-2\nu)r}\Big[(1-\nu)\Big(\frac{1}{r}\frac{\partial u}{\partial\theta}+\frac{1}{r}\frac{\partial^2 v}{\partial\theta^2}\Big)+\nu\frac{\partial^2 u}{\partial r\partial\theta}+\nu\frac{\partial^2 w}{\partial\theta\partial z}\Big]\\
&+\frac{E}{2(1+\nu)}\Big(\frac{\partial^2 v}{\partial z^2}+\frac{1}{r}\frac{\partial^2 w}{\partial\theta\partial z}\Big)+\frac{E}{(1+\nu)r}\Big(\frac{1}{r}\frac{\partial u}{\partial\theta}+\frac{\partial v}{\partial r}-\frac{v}{r}\Big)=0\\
&\frac{\partial E}{2(1+\nu)\partial r}\Big(\frac{\partial u}{\partial z}+\frac{\partial w}{\partial r}\Big)+\frac{E}{2(1+\nu)}\Big(\frac{\partial^2 u}{\partial r\partial z}+\frac{\partial^2 w}{\partial r^2}\Big)+\frac{E}{2(1+\nu)r}\Big(\frac{\partial^2 v}{\partial\theta\partial z}+\frac{1}{r}\frac{\partial^2 w}{\partial\theta^2}\Big)\\
&+\frac{E}{(1+\nu)(1-2\nu)}\Big[(1-\nu)\frac{\partial^2 w}{\partial z^2}+\nu\Big(\frac{1}{r}\frac{\partial u}{\partial z}+\frac{1}{r}\frac{\partial^2 v}{\partial\theta\partial z}\Big)+\nu\frac{\partial^2 u}{\partial r\partial z}\Big]\\
&+\frac{E}{2(1+\nu)r}\Big(\frac{\partial u}{\partial z}+\frac{\partial w}{\partial r}\Big)=0
\end{aligned}
\tag{2.5}
$$

In the present work, the heat conduction problem without the heat source is considered, and the heat balance equation for the corresponding steady state is defined as:

$$
\frac{1}{r}\frac{\partial}{\partial r}\Big(rK\frac{\partial T}{\partial r}\Big)+\frac{\partial}{\partial z}\Big(K\frac{\partial T}{\partial z}\Big)=0 \tag{2.6}
$$

It is noted that in the axisymmetric case, all field variables are independent of the circumferential direction θ, and there are only the radial and axial components of the displacement field, i.e. u and w, to be considered.

3. Thermo-mechanical boundary conditions

Mechanical and thermal boundary conditions of the shell for two cases of simply supported and clamped ends are described by the following relations:

$$
\begin{aligned}
&\text{Clamped:} && \text{at} && z=0,L: && u=v=w=T=0\\
&\text{Simply supported:} && \text{at} && z=0,L: && u=v=\sigma_z=T=0
\end{aligned}
\tag{3.1}
$$

where L is the length of the shell.

The inner and outer thermal and mechanical boundary conditions corresponding to the inner and outer radii of the cylindrical shell are defined according to the following relations, respectively

$$
\begin{aligned}
&\text{at} && r=a: && \sigma_r=P(\theta) && \tau_{rz}=\tau_{r\theta}=0 && T=0\\
&\text{at} && r=b: && \sigma_r=0 && \tau_{rz}=\tau_{r\theta}=0 && T=T_b
\end{aligned}
\tag{3.2}
$$

where for the axisymmetric problem, the radial stresses at the internal boundary are assumed to be zero, i.e. $P(\theta)=0$, and for the asymmetric case the radial stress is assumed to be a function of the circumferential coordinate, i.e. $P(\theta)=P_0\cos\theta$. As it is observed from Eqs. (3.2), for both cases the inner and outer boundaries are kept at constant temperatures of $T=0$ and $T=T_b$, respectively.

4. Differential quadrature formulation

In the present study, two types of differential quadratures are employed to approximate the first and the second order derivatives of the function; the polynomial expansion based differential quadrature for the radial and the longitudinal directions and the Fourier expansion based for the circumferential direction. The governing partial differential equations are discretized into the series form, using the differential quadratures.

4.1. Fourier expansion based differential quadrature (FDQ)

The desired function, i.e. $f(x)$, is approximated by a Fourier series expansion of the form

$$f(x) = c_0 + \sum_{k=1}^{N/2}(c_k \cos kx + d_k \sin kx) \tag{4.1}$$

where the function $f(x)$ constitutes an $N+1$ dimensional linear vector space V_{N+1}. Using these sets of base vectors, explicit formulations to compute the weighting coefficients of the first and the second order derivatives of the following forms are obtained (Shu, 2000)

$$\begin{aligned} &a_{ij} = \frac{q(x_i)}{2q(x_j)\sin\frac{x_i - x_j}{2}} \qquad q(x_i) = \prod_{k=0}^{N} \sin\frac{x_i - x_k}{2} \quad (i \neq j) \qquad a_{ii} = -\sum_{\substack{j=0 \\ i\neq j}}^{N} a_{ij} \\ &b_{ij} = a_{ij}\Big(2a_{ii} - \cot\frac{x_i - x_j}{2}\Big) \quad (i \neq j) \qquad b_{ii} = -\sum_{\substack{j=0 \\ i\neq j}}^{N} b_{ij} \end{aligned} \tag{4.2}$$

where a_{ij} and b_{ij} denote the weighting coefficients of the first and the second order derivatives of the function $f(x)$, respectively.

4.2. Polynomial based differential quadrature (PDQ)

Several polynomial differential quadrature methods are developed by researchers. In this work, the one that uses the following Lagrange interpolation polynomials as a test function is used (Shu, 2000)

$$f_k(x) = \frac{M(x)}{(x - x_k)M^{(1)}(x_k)} \qquad k = 1, 2, \ldots, N \tag{4.3}$$

where

$$M(x) = (x - x_1)(x - x_2)\cdots(x - x_N) \qquad M^{(1)}(x_i) = \prod_{\substack{k=1 \\ k\neq i}}^{N}(x_i - x_k) \tag{4.4}$$

By applying the above equation at N grid points, the following algebraic formulations to compute the weighting coefficients are developed (Shu, 2000)

$$a_{ij} = \frac{1}{x_j - x_i}\prod_{\substack{k=1 \\ k\neq i,j}}^{N}\frac{x_i - x_k}{x_j - x_k} \quad (i \neq j) \qquad a_{ii} = \sum_{\substack{k=1 \\ k\neq i}}^{N}\frac{1}{x_i - x_k} \qquad b_{ij} = \sum_{k=1}^{N} a_{ik}a_{kj} \tag{4.5}$$

4.3. Three-dimensional differential quadratures

The above differential quadrature approximation corresponds to a one-dimensional formulation. The differential quadrature approximation can be extended from the above formulation to other coordinates. The first order derivatives in the three-dimensional formulations can be approximated by

$$\left.\frac{\partial f}{\partial r}\right|_{ijk} \approx \sum_{l=1}^{N} A_{il}^{(1)} f_{ljk} \qquad \left.\frac{\partial f}{\partial \theta}\right|_{ijk} \approx \sum_{m=1}^{M} B_{jm}^{(1)} f_{imk} \qquad \left.\frac{\partial f}{\partial z}\right|_{ijk} \approx \sum_{n=1}^{P} C_{kn}^{(1)} f_{ijn} \tag{4.6}$$

And the second order derivatives are defined as

$$\begin{aligned}
&\left.\frac{\partial^2 f}{\partial r^2}\right|_{ijk} \approx \sum_{l=1}^{N} A_{il}^{(2)} f_{ljk} && \left.\frac{\partial^2 f}{\partial \theta^2}\right|_{ijk} \approx \sum_{m=1}^{M} B_{jm}^{(2)} f_{imk} \\
&\left.\frac{\partial^2 f}{\partial z^2}\right|_{ijk} \approx \sum_{n=1}^{P} C_{kn}^{(2)} f_{ijn} && \left.\frac{\partial^2 f}{\partial r \partial \theta}\right|_{ijk} \approx \sum_{l=1}^{N} A_{il}^{(1)} \sum_{m=1}^{M} B_{jm}^{(1)} f_{lmk} \\
&\left.\frac{\partial^2 f}{\partial r \partial z}\right|_{ijk} \approx \sum_{l=1}^{N} A_{il}^{(1)} \sum_{n=1}^{P} C_{kn}^{(1)} f_{ljn} && \left.\frac{\partial^2 f}{\partial \theta \partial z}\right|_{ijk} \approx \sum_{m=1}^{M} B_{jm}^{(1)} \sum_{n=1}^{P} C_{kn}^{(1)} f_{imn}
\end{aligned} \tag{4.7}$$

where $A^{(1)}$, $B^{(1)}$, $C^{(1)}$ and $A^{(2)}$, $B^{(2)}$, $C^{(2)}$ denote the weighting coefficients of the first and the second order derivatives of the function $f(r,\theta,z)$ with respect to the r, θ and z-directions respectively. N, M and P are the number of grid points chosen in the r, θ and z-directions, respectively. Using the differential quadrature method, the first governing equation in the radial direction is discretized, as follows

$$\begin{aligned}
&\frac{\partial E}{(1+\nu)(1-2\nu)\partial r}\left[(1-\nu)\sum_{l=1}^{N} A_{il}^{(1)} u_{ljk} + \nu\left(\frac{u_{ijk}}{r_i} + \frac{1}{r_i}\sum_{m=1}^{M} B_{jm}^{(1)} v_{imk}\right) + \nu\sum_{n=1}^{P} C_{kn}^{(1)} w_{ijn}\right] \\
&- \frac{\partial E}{(1-2\nu)\partial r}\alpha T_{ijk} + \frac{E}{(1+\nu)(1-2\nu)}\left[(1-\nu)\sum_{l=1}^{N} A_{il}^{(2)} u_{ljk} + \nu\left(\frac{1}{r_i}\sum_{l=1}^{N} A_{il}^{(1)} u_{ljk} - \frac{u_{ijk}}{r_i^2}\right.\right. \\
&\left.\left. + \frac{1}{r_i}\sum_{l=1}^{N}\sum_{m=1}^{M} A_{il}^{(1)} B_{jm}^{(1)} v_{lmk} - \frac{1}{r_i^2}\sum_{m=1}^{M} B_{jm}^{(1)} v_{imk}\right) + \nu\sum_{l=1}^{N}\sum_{n=1}^{P} A_{il}^{(1)} C_{kn}^{(1)} w_{ljnk}\right] \\
&- \frac{E\alpha}{1-2\nu}\sum_{l=1}^{N} A_{il}^{(1)} T_{ljk} - \frac{\partial \alpha}{(1-2\nu)\partial r} E T_{ijk} + \frac{E}{2(1+\nu)r_i}\left(\frac{1}{r_i}\sum_{m=1}^{M} B_{jm}^{(2)} u_{imk}\right. \\
&\left. + \sum_{l=1}^{N}\sum_{m=1}^{M} A_{il}^{(1)} B_{jm}^{(1)} v_{lmk} - \frac{1}{r_i}\sum_{m=1}^{M} B_{jm}^{(1)} v_{imk}\right) + \frac{E}{2(1+\nu)}\left(\sum_{n=1}^{P} C_{kn}^{(2)} u_{ijn}\right. \\
&\left. + \sum_{l=1}^{N}\sum_{n=1}^{P} A_{il}^{(1)} C_{kn}^{(1)} w_{ljnk}\right) + \frac{E}{(1+\nu)(1-2\nu)r}\left\{\left[(1-\nu)\sum_{l=1}^{N} A_{il}^{(1)} u_{ljk}\right.\right. \\
&\left. + \nu\left(\frac{u_{ijk}}{r_i} + \frac{1}{r_i}\sum_{m=1}^{M} B_{jm}^{(1)} v_{imk}\right) + \nu\sum_{n=1}^{P} C_{kn}^{(1)} w_{ijn}\right] - \left[(1-\nu)\left(\frac{u_{ijk}}{r_i} + \frac{1}{r_i}\sum_{m=1}^{M} B_{jm}^{(1)} v_{imk}\right)\right. \\
&\left.\left. + \nu\sum_{l=1}^{N} A_{il}^{(1)} u_{ljk} + \nu\sum_{n=1}^{P} C_{kn}^{(1)} w_{ijn}\right]\right\} + \rho r_i \omega^2 = 0
\end{aligned} \tag{4.8}$$

Derivatives of the elastic constant E and the thermal expansion coefficient α are defined according to their respective functions. The steady state temperature field is defined as

$$K\sum_{l=1}^{N} A_{il}^{(2)} T_{ljk} + \frac{K}{r_i}\sum_{l=1}^{N} A_{il}^{(1)} T_{ljk} + \frac{\partial K}{\partial r}\sum_{l=1}^{N} A_{il}^{(1)} T_{ljk} + K\sum_{n=1}^{P} C_{kn}^{(2)} T_{ijn} = 0 \tag{4.9}$$

where the derivative of K is obtained according to its respective function.

The stress boundary conditions are defined as

$$\begin{aligned}
&\frac{E}{(1+\nu)(1-2\nu)}\Big[(1-\nu)\sum_{l=1}^{N}A_{il}^{(1)}u_{ljk}+\nu\Big(\frac{u_{ijk}}{r_i}+\frac{1}{r_i}\sum_{m=1}^{M}B_{jm}^{(1)}v_{imk}\Big)+\nu\frac{\partial w}{\partial z}\Big]\\
&\quad-\frac{E}{(1-2\nu)}\alpha T_{ijk}-P(\theta)=0\\
&\frac{E}{2(1+\nu)}\Big(\frac{1}{r_i}\sum_{m=1}^{M}B_{jm}^{(1)}u_{imk}+\sum_{l=1}^{N}A_{il}^{(1)}v_{ljk}-\frac{1}{r_i}v_{ijk}\Big)=0\\
&\frac{E}{2(1+\nu)}\Big(\sum_{n=1}^{P}C_{kn}^{(1)}u_{ijn}+\sum_{l=1}^{N}A_{il}^{(1)}w_{ljk}\Big)=0
\end{aligned}\tag{4.10}$$

In order to proceed with numerical computations, sampling points in the radial and axial directions are defined using the Chebyshev polynomials, while for circumferential direction a uniform distribution is used. The coordinates of grid points used in the r, θ and z-directions are defined as follow

$$\begin{aligned}
r_{k_1}&=a+\frac{b-a}{2}\Big[1-\cos\Big(\frac{k_1-1}{N-1}\pi\Big)\Big] && k_1=1,\ldots,N\\
\theta_{k_2}&=2\pi\frac{k_2-1}{M} && k_2=1,\ldots,M\\
z_{k_3}&=\frac{L}{2}\Big[1-\cos\Big(\frac{k_3-1}{P-1}\pi\Big)\Big] && k_3=1,\ldots,P
\end{aligned}\tag{4.11}$$

5. Numerical results and discussions

At first, the results obtained are compared with the results reported for a thick hollow cylinder by Jabbari *et al.* (2002). It is assumed that the cylinder is made of materials graded along the r-coordinate. Variation of the modulus of elasticity E, the coefficient of thermal expansion α, and the thermal conduction coefficient K, are assumed to be obeying the following power law formulation

$$E(r)=E_i r^m \qquad \alpha(r)=\alpha_i r^m \qquad K(r)=K_i r^m \tag{5.1}$$

where E_i, α_i and K_i are the modulus of elasticity, the coefficient of thermal expansion and the thermal conduction coefficient at the inner radius.

The inner and the outer radii of the cylinder are assumed to be $a=1\,\mathrm{m}$ and $b=1.2\,\mathrm{m}$, respectively and the grading parameter m is chosen as 3. Poisson's ratio is assumed to be 0.3 and the modulus of elasticity and the thermal coefficient of expansion at the inner radius are $E_i=200\,\mathrm{GPa}$ and $\alpha_i=1.2\cdot10^{-6}\,/^{\circ}\mathrm{C}$, respectively. Temperature of the hollow cylinder at the inner and outer radii are assumed to be $T(a)=100^{\circ}\mathrm{C}$ and $T(b)=0^{\circ}\mathrm{C}$, respectively. The hollow cylinder is under the effect of an internal pressure of $50\,\mathrm{MPa}$, while the external pressure is zero, i.e. $\sigma_{rr}(a)=-50\,\mathrm{MPa}$ and $\sigma_{rr}(b)=0\,\mathrm{MPa}$.

Results of the convergence study for different grid numbers are shown in Figs. 2a,b. It is observed from Fig. 2a that by increasing the number of grid points, the results converge rapidly and the rate of convergence decreases as the number of grid points increases. Hence, an appropriate grid number of 20 is chosen. The radial distribution of the hoop stress and the radial displacement fields calculated by the present method are compared with the results reported by Jabbari *et al.* (2002) which indicate very good agreement, as shown in Figs. 2a and 2b.

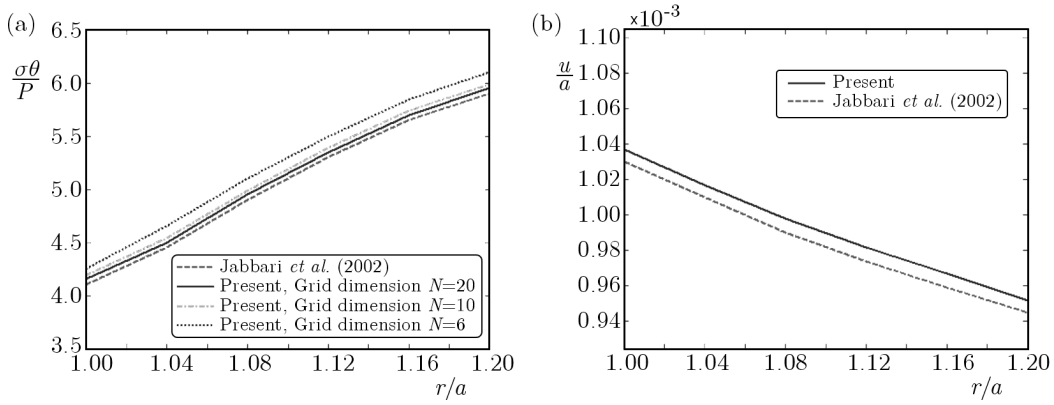

Fig. 2. Radial distribution of hoop stress (a), radial distribution of radial displacement (b) for an FGM cylindrical shell

5.1. Axisymmetric problem

In this section, numerical calculations for the hollow cylindrical shell made of an FG material, i.e. the outer surface made of Zirconia (ceramic) and the inner surface made of Aluminum (metal) are carried out. Properties of these materials are listed in Table 1 (Bayat *et al.* (2007)). For many engineering materials, the Poisson ratio is within the range of 0.25 to 0.35 and varies slightly. Hence, for simplicity, it is assumed that the Poisson ratio is constant as depicted in Table 1.

Table 1. Material properties

Material	E [GPa]	ν	α [10^{-6}/°C]	K [W/m°C]	ρ [kg/m^3]
Aluminum	70	0.3	23	209	2700
Zirconia	151	0.3	10	2	5700

A power law formulation is used to define the variation of material properties in the radial direction

$$Y(r) = Y_i\Big[1 - \Big(\frac{r-a}{b-a}\Big)^{\beta}\Big] + Y_o\Big(\frac{r-a}{b-a}\Big)^{\beta} \tag{5.2}$$

where Y_i and Y_o denote the material properties at the inner and the outer surfaces of the hollow cylindrical shell, respectively and β is the grading parameter describing the change of the volume fraction of two constituents. These properties include the elastic constant E, the coefficient of thermal expansion α, the thermal conduction coefficient K and the mass density ρ. Dimensionless results are obtained by defining the following dimensionless stresses, displacement and temperature fields

$$\begin{aligned} &\overline{\sigma}_{ij} = \frac{1-\nu}{E_0\alpha_0 T_0 + (1-\nu)\rho_0\omega_0^2 b^2}\sigma_{ij} \qquad && \overline{T} = \frac{T}{T_o} \\ &\overline{u} = \frac{E_0}{(1+\nu)[E_0\alpha_0 T_0 + (1-\nu)\rho_0\omega_0^2 b^2]b}u \end{aligned} \tag{5.3}$$

It should be noted that all numerical results are calculated and presented for the midpoint, i.e. $z = L/2$, of the cylindrical shell with clamped boundary conditions at two ends, as defined in Eq. $(3.1)_1$. For the axisymmetric case, variations of parameters i.e. the stresses, radial displacement and temperature of the midpoint along the radial direction are shown while for the asymmetric case, variations of the parameters related to mid-plane along the circumferential direction are presented.

An FG shell rotating at $\omega = 500\,\mathrm{rad/s}$ and subjected to a thermal loading of $T(a) = 0°\mathrm{C}$ and $T(b) = 100°\mathrm{C}$ at the inner and outer boundaries respectively, is considered. The effect of β on the variation of stresses, radial displacement and temperature distributions are examined first and the results are shown in Fig. 3. It is observed from Fig. 3a that the dimensionless radial stress reaches zero at the inner and outer surfaces and the maximum dimensionless radial stress decreases as β increases. Moreover, maximum values occur at certain internal positions which shift toward the outer surface as β increases. Such a trend is also found with the value of the dimensionless circumferential stress, as depicted in Fig. 3b. It is observed from Fig. 3c that the dimensionless axial stress reduces as β increases. For the case of $\beta = 10$, the rate of change of the dimensionless circumferential and axial stresses at the interior sections of the structure is lower than at the sections adjacent to the inner and the outer boundaries. It is revealed from Fig. 3d that the dimensionless shear stress reaches zero at the inner and outer surfaces, satisfying the boundary conditions. As β increases, values of the dimensionless shear stress decrease in magnitude. The influence of β on the dimensionless radial displacement is shown in Fig. 3e indicating a monotonous decrease with the increase of β. The maxima of the dimensionless radial displacement for linearly varying material properties occur at the outer surface. As it is expected from Fig. 3f, the distribution of temperature in the shell is nonlinear, due to the power law variation of the thermal conductivity across the thickness.

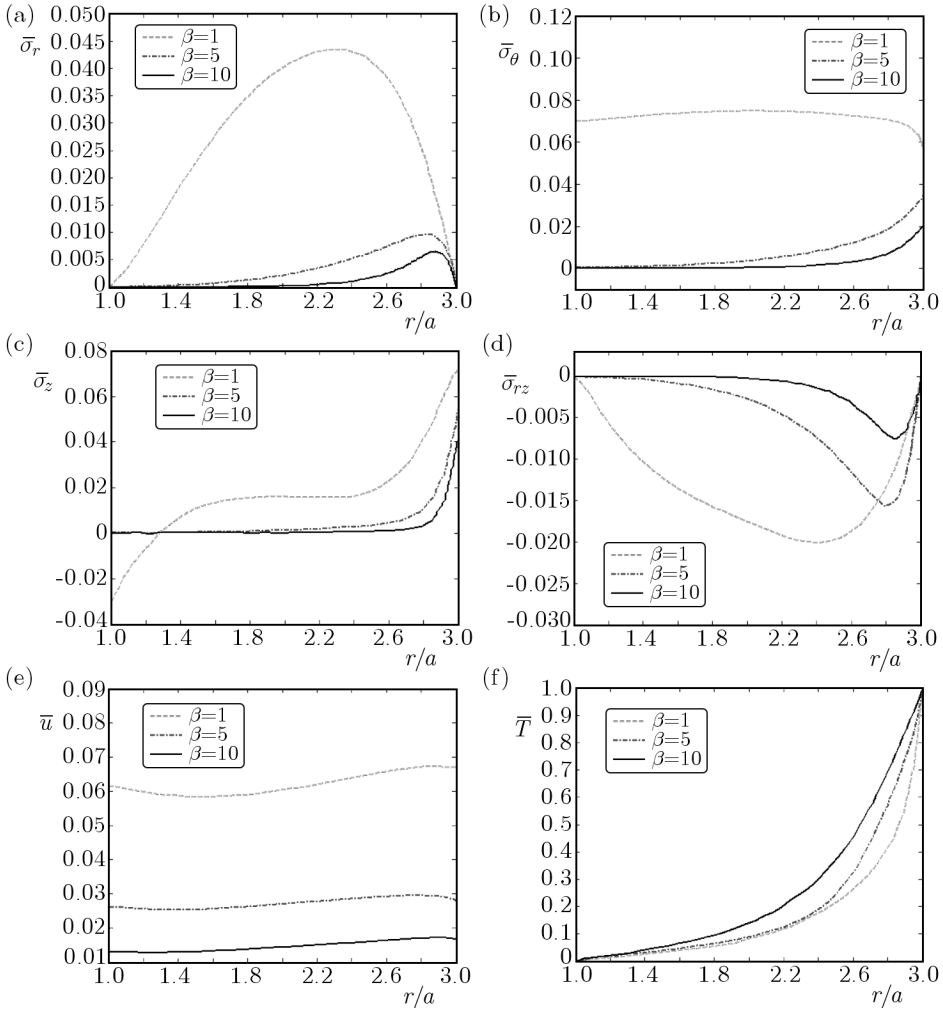

Fig. 3. Effects of β on the (a) radial stress, (b) circumferential stress, (c) axial stress, (d) shear stress, (e) radial displacement, (f) temperature distribution

The effects of temperature difference at two surfaces of the cylindrical shell on the dimensionless stresses and radial displacement are demonstrated in Figs. 4a-4e. For the sake of simplicity, numerical calculations are carried out with the temperature of the inner surface being fixed, i.e. $T(a) = 0°\mathrm{C}$, with the temperature at the outer surface of the cylindrical shell varying as a parameter. The material properties are assumed to vary linearly in the radial direction, i.e. $\beta = 1$ and the cylindrical shell is assumed to be rotating at a constant angular velocity of $\omega = 500\,\mathrm{rad/s}$. It is observed from Fig. 4a that the dimensionless radial stress increases with a slow rate as the temperature difference increases and the location of its maxima shifts toward the outer surface of the cylinder. It is expected that at low temperature difference, the induced stresses and deformations are mainly due to the centrifugal force and not the temperature difference. Variations of the dimensionless circumferential and axial stresses are shown in Figs. 4b and 4c respectively, which indicate that these stresses tend towards the compressive region and their absolute values increase as the temperature difference increases. It is also realized from Fig. 4d that the absolute value of the dimensionless shear stress increases as the temperature difference increases. Variation of the dimensionless radial displacement with temperature difference at boundaries is displayed in Fig. 4e. It is also revealed from Figs. 4a to 4e that the dimensionless stresses and the radial displacement are sensitive to the applied thermal loading.

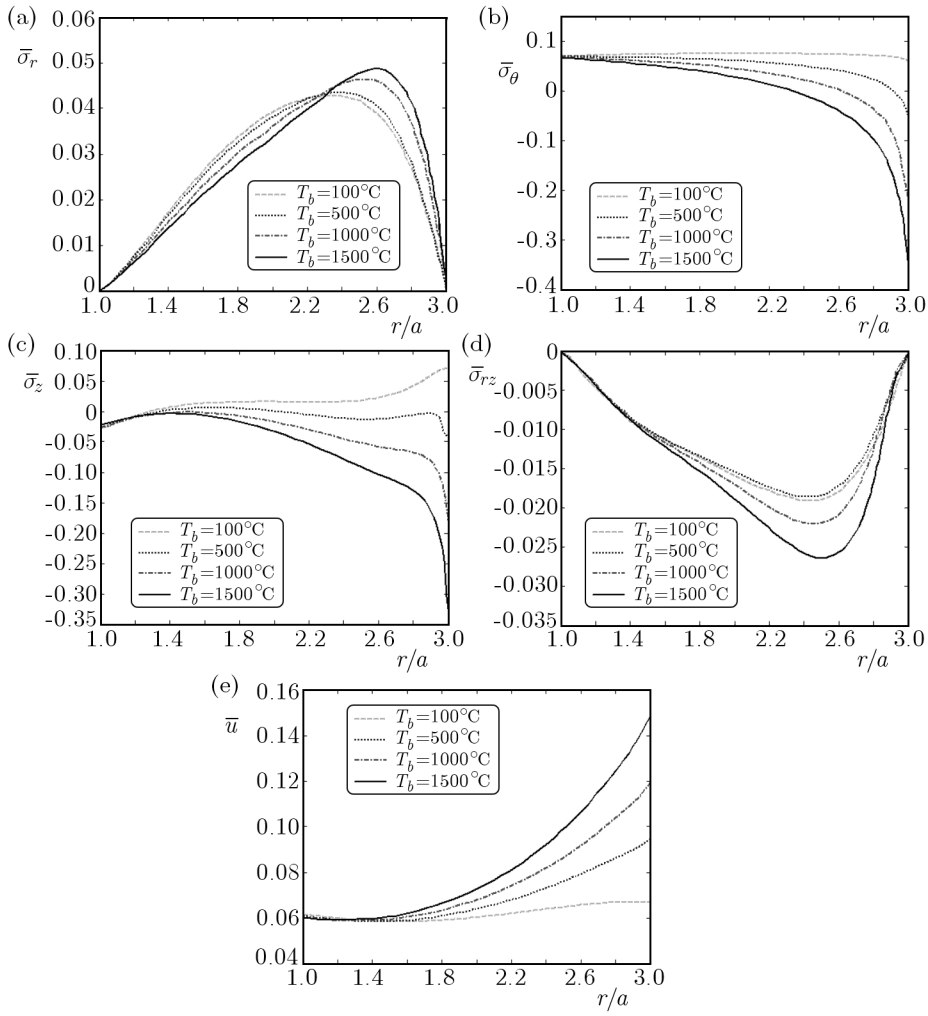

Fig. 4. Effects of T_b on the (a) radial stress, (b) circumferential stress, (c) axial stress, (d) shear stress, (e) radial displacement

As the last case of an axisymmetric problem, the effect of boundary condition, i.e. simply supported or clamped at two ends, is investigated and the results are plotted in Figs. 5a-5e. In this section the cylindrical shell with linearly varying material properties rotating at a constant angular speed of $\omega = 500\,\mathrm{rad/s}$ and subjected to a thermal boundary condition of $T(a) = 0°\mathrm{C}$ and $T(b) = 100°\mathrm{C}$ is considered. It is revealed from Figs. 5a-5d that the pattern of dimensionless stresses are similar for both boundary conditions, however the maximum values of the dimensionless stresses for the simply supported boundary condition is higher than those of the clamped one. It is noted from Fig. 5e that for simply supported boundary conditions at $z = 0, L$, the variation amplitude of the curve of the radial displacement becomes higher than that the clamped condition.

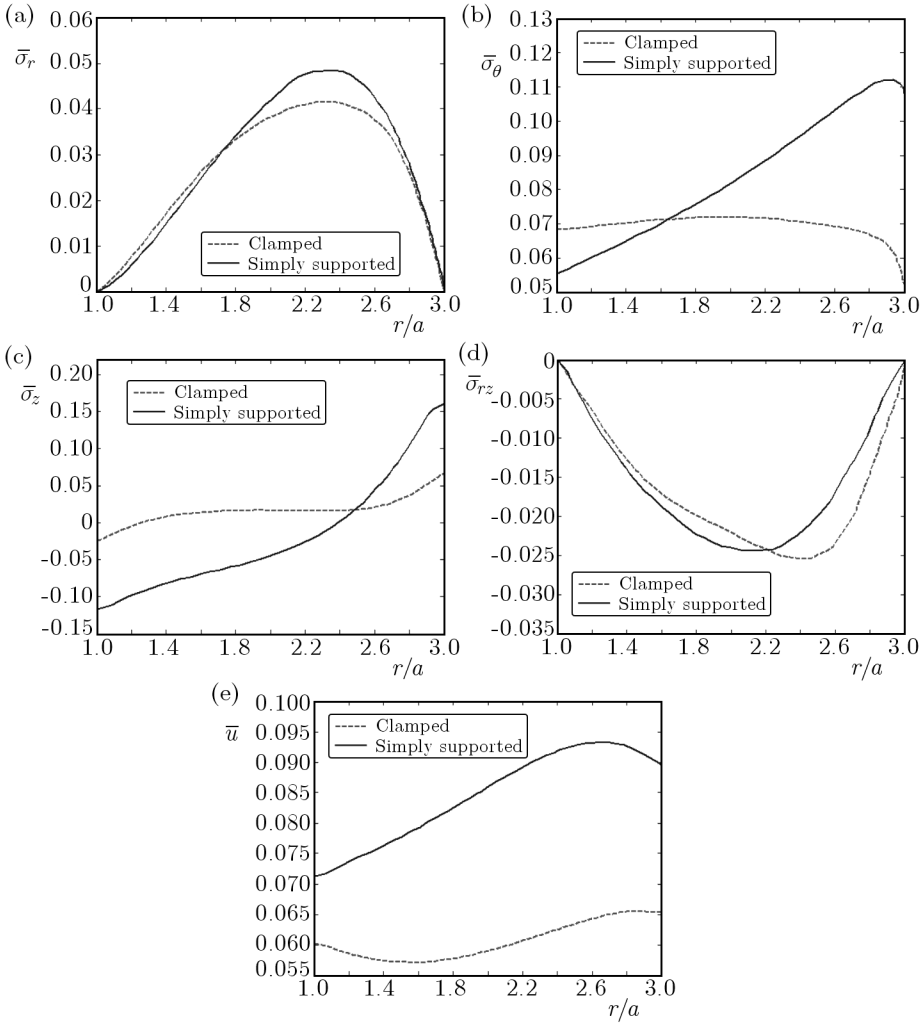

Fig. 5. Effects of the boundary condition on the (a) radial stress, (b) circumferential stress, (c) axial stress, (d) shear stress, (e) radial displacement

5.2. Asymmetric problem

For the asymmetric problem, it is assumed that the cylindrical shell is subjected to a cosine type of internal pressure loading, i.e. $P(\theta) = P\cos(\theta)$. Effects of ω on the distributions of the dimensionless stresses and the radial displacement of the mid-plane of the cylindrical shell with linearly varying material properties and thermal boundary conditions of $T(a) = 0°\mathrm{C}$ and $T(b) = 100°\mathrm{C}$ are presented in Figs. 6a to 6e. The dimensionless radial, circumferential

and axial stresses increase with the increase in ω showing high dependency on the angular velocity; however, the dimensionless shear stress remains nearly constant. It is also noted that the dimensionless radial displacement increases as ω increases.

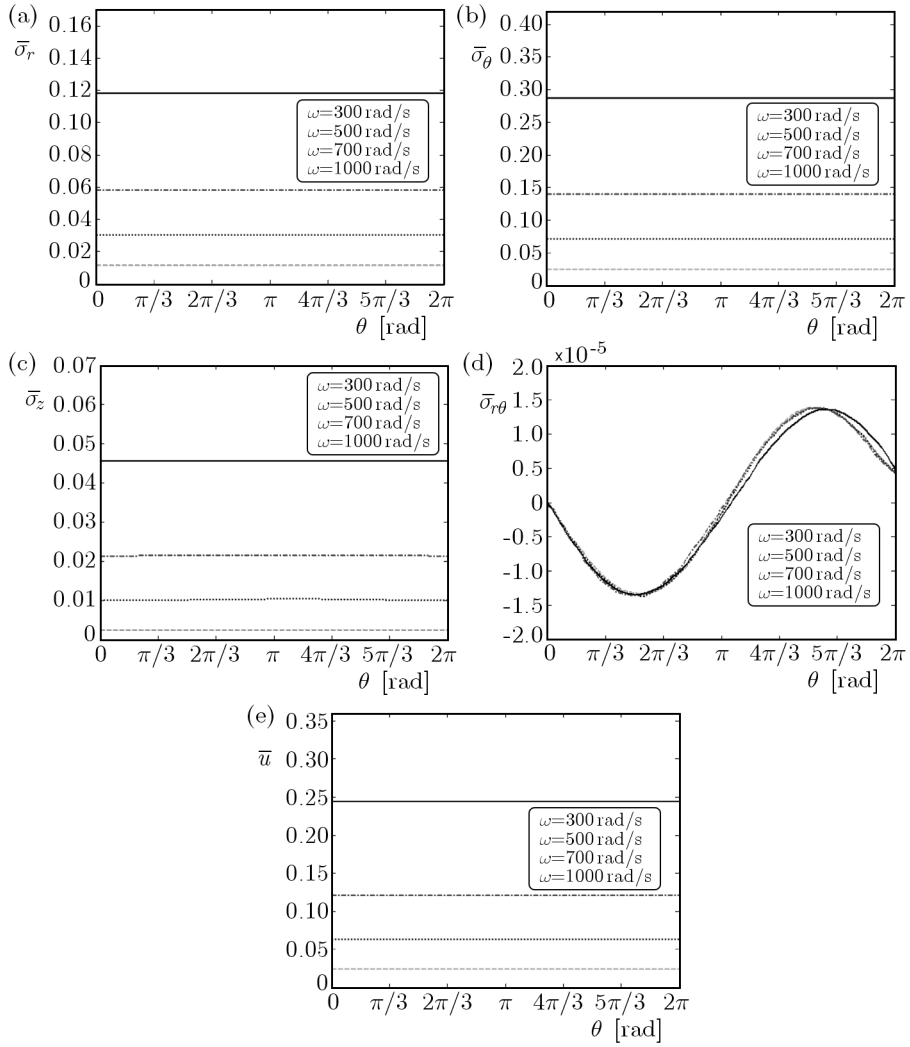

Fig. 6. Effects of ω on the (a) radial stress, (b) circumferential stress, (c) axial stress, (d) shear stress, (e) radial displacement

The effects of temperature difference on the stresses and radial displacement at the mid-plane of the shell are calculated and shown in Figs. 7a-7e. The temperature of the inner surface is assumed to be constant (i.e. $T(a) = 0°\mathrm{C}$) and the temperature at the outer surface varying as a parameter, as in the case of the axisymmetric problem. Linearly varying material properties and $\omega = 500\,\mathrm{rad/s}$ are assumed. As the temperature difference increases, the dimensionless radial stress and displacement increase, however the dimensionless circumferential and shear stresses decrease. It is observed that variations of the dimensionless shear stress are negligible indicating that the temperature difference has higher effect on the normal stresses in the r, θ and z-direction and has negligibly small effect on the shear stress.

Finally, the effect of the thickness on the dimensionless stresses and the radial displacement are investigated. In this calculation, parameters are chosen as $\beta = 1$, $T(a) = 0°\mathrm{C}$ and $T(b) = 100°\mathrm{C}$ and $\omega = 500\,\mathrm{rad/s}$. The dimensionless stresses, radial displacement and temperature distributions for different ratios of the outer radius to the inner radius of the cylindrical shell equal to $b/a = 3$, 6, 9, 12 are shown in Figs. 8a-8e. As it is expected, values of the dimensionless stresses and radial displacement become lower as the hollow cylindrical shell becomes thicker.

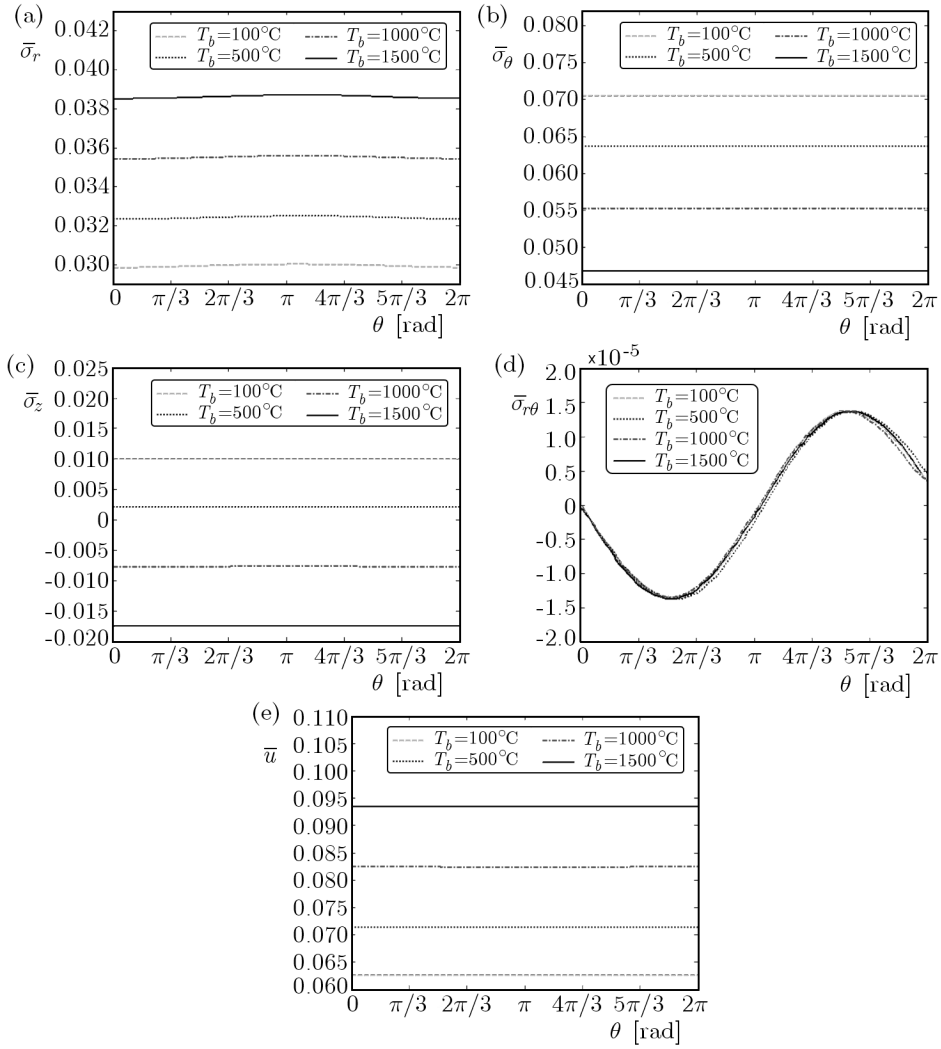

Fig. 7. Effects of T_b on the (a) radial stress, (b) circumferential stress, (c) axial stress, (d) shear stress, (e) radial displacement

6. Conclusions

In this paper, a numerical method to solve the thermo-elastic problem of a rotating hollow cylindrical shell made of an FG material is presented. Governing differential equations were rewritten with the help of the Fourier and polynomial differential quadratures and solved numerically with complete satisfaction of all boundary conditions. The distributions of dimensionless stresses, radial displacement and temperature fields of the rotating shell for various boundary conditions, material properties, angular velocities and temperature differences are calculated and presented.

From the present study, the following conclusions are obtained:

A – Axisymmetric loading and boundary conditions

- The dimensionless stresses and radial displacement decrease and the dimensionless temperature distribution increases in magnitude as the gradient parameter β increases.
- The maximum value of the dimensionless radial stress increases as the temperature difference increases.

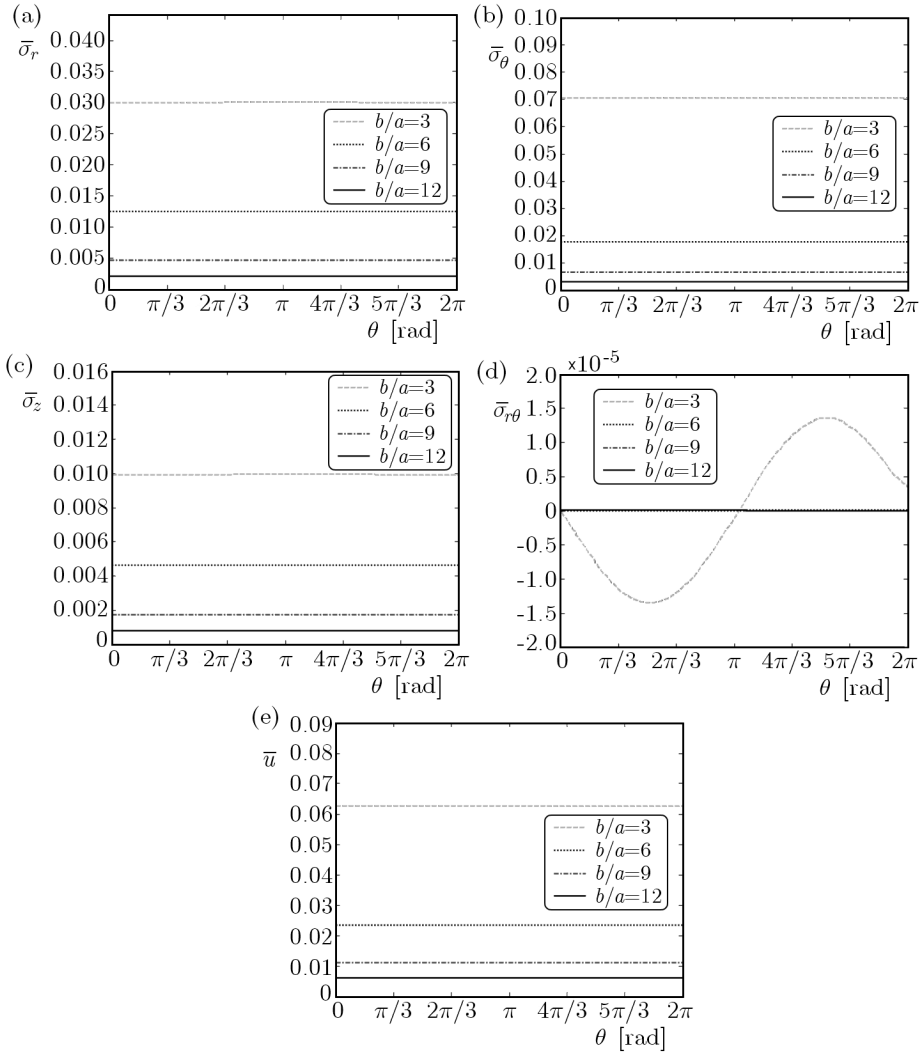

Fig. 8. Effects of b/a on the (a) radial stress, (b) circumferential stress, (c) axial stress, (d) shear stress, (e) radial displacement

- The maximum values of stresses and displacement in shells with simply supported end boundary conditions are higher than those with clamped boundary conditions.
- In an FG shell with a power law variation of properties, the distribution of temperature through thickness of the shell is nonlinear.

B – Asymmetric loading and boundary conditions

- The dimensionless radial, circumferential and axial stresses and radial displacement at the mid-plane along the circumference increase as ω increases, indicating strong dependency of these stresses on the angular velocity, however the dimensionless shear stress is almost constant.
- The dimensionless radial stress and displacement at the mid-plane along the circumference increase, while the dimensionless circumferential and axial stresses decrease as the temperature difference increases.
- As the hollow cylindrical shell becomes thicker, values of the dimensionless stresses and radial displacement at the mid-plane along the circumference become smaller.

References

1. Afsar A.M., Go J., 2010, Finite element analysis of thermoelastic field in a rotating FGM circular disk, *Applied Mathematical Modelling*, **34**, 3309-3320

2. Akbari Alashti R., Khorsand M., 2011, Three-dimensional thermo-elastic analysis of a functionally graded cylindrical shell with piezoelectric layers by differential quadrature method, *International Journal of Pressure Vessels and Piping*, **88**, 167-180

3. Arciniega R.A., Reddy J.N., 2007, Large deformation analysis of functionally graded shells, *International Journal of Solids and Structures*, **44**, 2036-2052

4. Bahtui A., Eslami M.R., 2007, Coupled thermoelasticity of functionally graded cylindrical shells, *Mechanics Research Communications*, **34**, 1-18

5. Bayat M., Saleem M., Sahari B.B., Hamouda A.M.S., Mahdi E., 2007, Thermo elastic analysis of a functionally graded rotating disk with small and large deflections, *Thin-Walled Structures*, **45**, 677-691

6. Shu C., 2000, *Differential Quadrature and its Application in Engineering*, Springer-Verlag, London

7. Hojjati M.H., Jafari S., 2008, Semi-exact solution of elastic non-uniform thickness and density rotating disks by homotopy perturbation and Adomian's decomposition methods, Part I: Elastic solution, *International Journal of Pressure Vessels and Piping*, **85**, 871-878

8. Jabbari M., Sohrabpour S., Eslami M.R., 2002, Mechanical and thermal stresses in a functionally graded hollow cylinder due to radially symmetric loads, *International Journal of Pressure Vessels and Piping*, **79**, 493-497

9. Koizumi M., 1993, The concept of FGM, [In:] *Ceramic Transactions. Functionally Gradient Materials*, Holt J.B., Koizumi M., Hirai T., Munir Z.A. (Editors), American Society, **34**, 3-10

10. Matsunaga H., 2009, Stress analysis of functionally graded plates subjected to thermal and mechanical loadings, *Composite Structures*, **87**, 344-357

11. Pelletier J.L., Vel S.S., 2006, An exact solution for the steady-state thermoelastic response of functionally graded orthotropic cylindrical shells, *Original Research Article International Journal of Solids and Structures*, **43**, 1131-1158

12. Peng X.-L., Li X.-F., 2010, Thermal stress in rotating functionally graded hollow circular disks, *Composites Structures*, **92**, 1896-1904

13. Shahzamanian M.M., Sahari B.B., Bayat M., Mustapha F., Ismarrubie Z.N., 2010, Finite element analysis of thermoelastic contact problem in functionally graded axisymmetric brake disks, *Composite Structures*, **92**, 1591-1602

14. Sofiyev A.H., 2007, Thermoelastic stability of functionally graded truncated conical shells, *Composite Structures*, **77**, 56-65

15. Suresh S., Mortensen A., 1998, *Fundamentals of Functionally Graded Materials*, Institute of Materials (IOM), Communications Limited, London

16. Wu L., Jiang Z., Liu J., 2005, Thermoelastic stability of functionally graded cylindrical shells, *Composite Structures*, **70**, 60-68

17. Zhao X., Liew K.M., 2011, Free vibration analysis of functionally graded conical shell panels by a meshless method, *Composite Structures*, **93**, 649-664

Trójwymiarowa analiza asymetrycznie termosprężystego zagadnienia wirującej powłoki cylindrycznej wykonanej z materiału gradientowego

Streszczenie

W pracy zaprezentowano analizę asymetrycznej deformacji i naprężeń w otwartej powłoce cylindrycznej wykonanej z materiału gradientowego i poddanej obciążeniom termosprężystym. Do badań wykorzystano metodę kwadratury różniczkowej. Nie tracąc na ogólności rozważań, założono, że właściwości materiału zmieniają się stopniowo w kierunku promieniowym zgodnie z przyjętym prawem potęgowym. Przyjęto ponadto, że współczynnik Poissona jest stały. Cząstkowe równania różniczkowe modelu wyrażono w funkcji przemieszczenia i pola temperatur ujętych w formie szeregów uzyskanych za pomocą dwóch wersji metody kwadratury różniczkowej, tj. kwadratury Fouriera i wielomianowej. Powłokę cylindryczną badano dla osiowo-symetrycznego i asymetrycznego stanu obciążenia. Wyniki symulacji numerycznych dla stanu osiowo-symetrycznego porównano z rozwiązaniami ścisłymi, stwierdzając bardzo dobrą zgodność. Przedstawiono także wyniki analizy termosprężystości dla przypadku asymetrycznego powłoki wirującej ze stałą prędkością kątową. Przedyskutowano ponadto wpływ wykładnika potęgowego rozkładu gradientowego właściwości materiału, wpływ prędkości wirowania, różnic temperatury i geometrii na przemieszczenia promieniowe powłoki i kształt pola cieplnego.

Manuscript received December 12, 2011; accepted for print April 15, 2012